Micro structure and strain relaxation in thin nanocrystalline platinumfilms produced via different sputtering techniques

Gruber, W.; Baehtz, C.; Horisberger, M.; Ratschinski, I.; Schmidt, H.;

Originally published:

February 2016

Applied Surface Science 368(2016), 341-347

DOI: https://doi.org/10.1016/j.apsusc.2016.02.015

Perma-Link to Publication Repository of HZDR:

https://www.hzdr.de/publications/Publ-25011

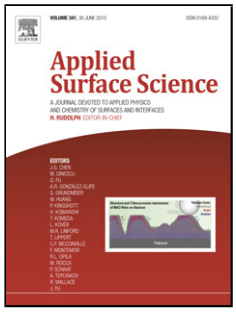

Title: Micro structure and strain relaxation in thin nanocrystalline platinum films produced via different sputtering techniques

Author: Wolfgang Gruber Carsten Baehtz Michael Horisberger Ingmar Ratschinski Harald Schmidt

PII: S0169-4332(16)30162-3
DOI: http://dx.doi.org/doi:10.1016/j.apsusc.2016.02.015
Reference: APSUSC 32533

To appear in: *APSUSC*

Received date: 5-10-2015
Revised date: 11-1-2016
Accepted date: 1-2-2016

Please cite this article as: W. Gruber, C. Baehtz, M. Horisberger, I. Ratschinski, H. Schmidt, Micro structure and strain relaxation in thin nanocrystalline platinum films produced via different sputtering techniques, *Applied Surface Science* (2016), http://dx.doi.org/10.1016/j.apsusc.2016.02.015

Highlights

- Residual strain relaxation in nano crystalline platinum films was investigated.
- Magnetron sputtered and ion beam sputtered Pt films are compared.
- XRD measurements were carried out using synchrotron radiation.
- Thickness fringes in the Bragg peak give information on microstructure.
- Residual strain relaxation is stronger in films composed of equally oriented columns.

Graphical abstract

Micro structure and strain relaxation in thin nanocrystalline platinum films produced via different sputtering techniques

Wolfgang Gruber[*,a], Carsten Baehtz[b], Michael Horisberger[c], Ingmar Ratschinski[d,e] and Harald Schmidt[a,e]

[a] Institut für Metallurgie, TU Clausthal, Robert-Koch-Str. 42, D38678 Clausthal-Zellerfeld, Germany

[b] Institut für Ionenstrahlphysik und Materialforschung, Helmholtz-Zentrum Dresden-Rossendorf, Dresden, Germany

[c] Laboratory for Scientific Developments & Novel Materials (LDM), Paul-Scherrer-Institute, Villigen PSI, Switzerland

[d]Institut für Nichtmetallische Werkstoffe, TU Clausthal, Zehntnerstr. 2a, D-38678 Clausthal-Zellerfeld, Germany

[e] Clausthaler Zentrum für Materialtechnik, Leibnizstraße 9, D-38678 Clausthal-Zellerfeld, Germany

[*]Corresponding author

Keywords: nanocrystalline platinum films; strain relaxation; thickness fringes

Abstract

In this study we investigated the correlation between microstructure and residual strain relaxation in nanocrystalline Pt films with a thickness of about 20 nm produced by different deposition techniques: magnetron sputtering and ion beam sputtering. X-ray diffractometry was carried out using synchrotron radiation. The out-of-plane interplanar distance was measured during isothermal in situ annealing at temperatures between 130 °C und 210 °C. The thermoelastic expansion coefficient is equal for both types of nanocrystalline Pt films and

slightly lower than for coarse grained Pt. The relaxation of residual out-of-plain strain depends on temperature and is significantly stronger in the case of the magnetron sputtered films than for the ion beam sputtered films. Different relaxation of compressive stress is ascribed to the different microstructures which evolve during deposition via the corresponding deposition technique. Thickness fringes around the (111) Bragg peak deposited via magnetron sputtering reveal that these films are essentially composed of columnar (111) oriented grains which cover the whole film thickness. In contrast, no thickness fringes are observed around the (111) Bragg peak of films prepared by ion beam sputtering indicating a significantly different microstructure. This is confirmed by Electron Backscatter Diffraction which reveals a (111) texture for both types of films. The (111) texture, however, is significantly stronger in the case of the magnetron sputtered films. Grain growth at low homologous temperatures is considered to be an important contribution to relaxation of residual stress.

1. Introduction

In the present work we investigate residual strain relaxation of thin Pt films deposited by different deposition techniques: magnetron sputtering and ion beam sputtering. Residual stress and strain are typical characteristics of film substrate combinations. The origin of residual stress in thin metal films is widely discussed in literature [1-7]. Metal films are commonly assumed to develop via Vollmer-Weber growth mode [7]. At the beginning of deposition discrete islands of the metal are built on the substrate. With increasing deposition time the islands grow. Growth of the islands adhered to the substrate is associated with stress which is commonly compressive [4-6]. After impingement, coalescence of the islands takes place: the island built a grain boundary to reduce the surface. Coalescence is associated with tensile stress [8]. Further deposition leads to a continuous film. The residual stress of the final film can be either tensile or compressive and depends on the deposition conditions [9]. On one hand, post- annealing of the metal films adhered to the substrate induces thermal stress. On

the other hand, relaxation processes of the intrinsic (growth related) stresses can take place since thermal energy is available.

In the present work, we deposited Pt films with a final thickness of about 20 nm using magnetron sputtering or ion beam sputtering. The residual stress of the as-deposited films is compressive for both deposition techniques. After deposition we performed X-ray diffraction measurements (XRD) during in situ annealing. The out-of-plane interplanar distance was determined for the Pt films as-deposited, during in situ annealing and after cooling down to room temperature. From the diffractograms information on the microstructure and the change of the microstructure during in situ annealing is deduced. The amount of residual strain which is released during in situ annealing at a given temperature is significantly different for the two types of Pt films. Release of residual strain is related to the microstructure.

2. Experimental

Ion beam sputtered Pt films with were deposited in argon using a commercial ion beam coater (Gatan IBC 651) at 5 keV and a working pressure of 0.5 Pa (base pressure < 5×10^{-4} Pa). The deposition rate was 0.7 nm/min and the thickness of the films was about 20 nm. Magnetron sputtered films were prepared at the Paul Scherrer Institute (PSI), Switzerland, using dc magnetron sputtering. Here, sputtering was carried out in an argon atmosphere at a power of 50W and a working pressure of 0.3 Pa (base pressure < 4×10^{-4} Pa). The deposition rate was 0.5 nm/s and the thickness of the films was about 20 nm. Commercially available oxidized silicon wafers were used as substrates in order to impede silicide formation during post-annealing. During deposition the substrates were at room temperature. The thickness of the films was measured using X-ray reflectometry.

XRD experiments in $\Theta/2\Theta$ geometry were carried out at the Rossendorf beam line at ESRF (BM20), Grenoble, using a six-circle goniometer (HUBER) and a parallel beam. The X-ray

energy was 11500 eV corresponding to a wave length of 1.08 Å. The samples were placed on a heater. Sample temperature was measured using a type K thermocouple mounted at the sample surface. Temperature was controlled using a Eurotherm 2804 temperature controller. Sample and heater were inside a Kapton dome which was evacuated. During heating a vacuum of about 4×10^{-4} Pa was achieved. Rocking curves and z-scans were measured to align the sample. Afterwards XRD was measured for the as-deposited sample. After heating up the sample was aligned again and XRD was measured. During in situ annealing alignment and XRD measurement were alternately repeated. After cooling down to room temperature the sample was aligned again and XRD was measured. The successive alignment was indispensable in order to obtain reliable measurements. Since the beam current at the synchrotron varies with time the intensity of the primary X-ray beam is monitored at the beamline. In order to compare the intensities of the Bragg peaks measured during a beam time the diffractograms were normalised to the monitor count rate. During beam time the settings of the monitor are unchanged. However, the intensities of Bragg peaks measured at different beam times cannot be compared directly due to different operation modes.

Electron Backscatter Diffraction (EBSD) measurements were carried out using a Nordlys EBSD detector of Oxford Instruments installed in a FEI Helios NanoLab 600. For these measurements four samples were investigated at a working distance of 10 mm and a specimen tilt of 71° at an acceleration voltage of 20 kV and a beam current of 1.4 nA. The EBSD system was calibrated by means of a single crystalline silicon sample. The data were recorded and processed using the CHANNEL5 suite of Oxford instruments. Inverse pole figures were calculated for each sample based on EBSD mappings of 10000 points.

3. Results

As mentioned, XRD was measured in Θ/2Θ geometry. In this geometry only atomic planes parallel to the sample surface contribute to the diffractograms. This means that the out-of-

plane interplanar distance is probed. We measured the (111) Bragg peak which is by far the strongest peak in the diffractograms. Fig. 1a shows Bragg peaks of a Pt film with a thickness of about 20 nm deposited via magnetron sputtering. The solid line is the Bragg peak of the Pt film as-deposited and the dotted line is the Bragg peak of the Pt film after annealing at 180 °C for 10 h and cooling down to room temperature. The intensity of the Bragg peak is significantly increased after annealing (note the logarithmic scale). The peak position is shifted to a higher 2Θ value. This means that the out-of-plane interplanar distance is decreased. The Bragg peaks are asymmetric and show characteristic interference fringes. These thickness fringes arise if a film is composed of columnar grains with uniform size and orientation. The fringes are already present in the Bragg peak of the as-deposited film and are much more pronounced after annealing. To determine the out-of-plan interplanar distance we fitted the peaks using a split pseudo-Voigt function and calculated it from the peak position using Bragg's law. Fig. 1b shows the corresponding Bragg peaks of a 20 nm Pt film deposited via ion beam sputtering in the as-deposited state (solid line) and after annealing at 180 °C for 10 h and cooling down to room temperature (dotted line). Since the measurements for the two types of films were performed at different beam times the intensities cannot be compared directly and are given in arbitrary units (see section 2). In contrast to the magnetron sputtered film, no fringes can be observed at all around the Bragg peaks of the ion beam sputtered film. The intensity of the Bragg peak is only slightly increased but the peak position is also shifted to a higher 2Θ value. This shift, however, is significantly smaller than in the case of the magnetron sputtered Pt film.

During heating up the sample the out-of-plane interplanar distance of the Pt films is expected to increase due to thermal expansion. However, the films are attached to the substrate. The thermal expansion coefficient of Pt is significantly higher than the thermal expansion coefficient of the substrate (see below). Therefore, additionally to the thermal expansion the out-of-plane interplanar distance is increased due to the increasing compressive stress parallel

to the film surface arising from the different thermal expansion coefficients. Thermal expansion and strain due to changing compressive stress are referred to as thermoelastic expansion.

However, if thermal energy is available, stress relaxation processes can also take place during annealing, which are expected to reduce the out-of-plane interplanar distance. Fig. 2a shows the out-of-plane interplanar distance with respect to the in situ annealing time for magnetron sputtered films annealed at 130 °C and 180 °C, respectively. At a temperature of 130 °C after 10 minutes of annealing the out-of-plane interplanar distance is increased compared to the value at room temperature due to thermoelastic expansion. For longer annealing times, the interplanar distance decreases successively due to relaxation processes. At 180 °C after 10 minutes of annealing the out-of-plane interplanar distance is smaller than for the sample as-deposited. This means that thermoelastic expansion is over compensated due to the relaxation processes and the out-of-plane interplanar distance decreases continuously from the beginning. A stronger relaxation effect at higher temperatures indicates that the relaxation process is thermally activated. For the ion beam sputtered samples the situation is similar (Fig. 2b). However, at a given temperature and annealing time the change of the out-of-plane interplanar distance is significantly smaller than in the case of the magnetron sputtered Pt films compared to the respective values of the as-deposited samples.

During in situ annealing the out-of-plane interplanar distance relaxes until an approximately constant value is reached (Fig. 2). We can determine the thermoelastic expansion coefficient, α_{thel}, from the difference of the fully relaxed out-of-plane interplanar distance (the last measured value at temperature T) and the out-of-plane interplanar distance measured after cooling down to room temperature according to

$$\varepsilon_{thel} = \frac{d_{rel}(T) - d_{RT}}{d_{RT}} = \alpha_{thel}\Delta T, \qquad (1)$$

where ε_{thel} is the thermoelastic strain, d_{rel} is the fully relaxed out-of-plane interplanar distance (the last measured value at temperature T), d_{RT} the out-of-plane interplanar distance after cooling down to room temperature and ΔT the temperature difference to room temperature. By heating up again the sample under investigation, it is proven that thermoelastic expansion is reversible for the relaxed films (not shown). In Fig. 3 the thermoelastic expansion of the ion beam sputtered samples and the magnetron sputtered samples is plotted with respect to the temperature difference, ΔT. The data were fitted under the constraint $(d_{rel}(T) - d_{RT})/d_{RT} = 0$ for $\Delta T = 0$. Within error limits the thermoelastic expansion coefficient is equal for both types of samples. The mean value for the thermoelastic expansion coefficient is $(1.33 \pm 0.02) \times 10^{-5}$ K^{-1}.

If the sample is annealed the expansion of the Pt film perpendicular to the surface is the sum of the thermal expansion of the Pt film and the elastic expansion which arises from the different thermal expansion coefficients of film and substrate. This elastic expansion is proportional to the difference of the thermal expansion coefficients of film and substrate. The expected thermoelastic expansion coefficient for a Pt film deposited on SiO_2 can be determined from literature data. The thermal expansion coefficients are $\alpha = 9\times10^{-6}$ K^{-1} for Pt [10] and $\alpha_S = 0.6\times10^{-6}$ K^{-1}[11] for SiO_2. Therefore, a thermoelastic expansion coefficient of $[2\nu/(1 - \nu) + 1]\alpha - 2\nu/(1 - \nu)\alpha_s = 1.97\times10^{-5}$ is expected ($\nu = 0.39$ [12] is the Poisson number). Consequently, the thermoelastic expansion coefficient of the sputter deposited nanocrystalline Pt films investigated in this work (Fig. 3) is lower than the theoretical value expected for coarse grained samples or single crystals. We tentatively attribute this to the different nano/micro structure.

4. Discussion

During heating up the sample to a certain temperature T, relaxation processes are initiated while the equilibrium temperature is reached and sample alignment is completed. Therefore,

we cannot directly measure the out-of-plane interplanar distance at temperature T for the annealing time $t = 0$, $d(T,0)$, which is the reference value for the residual strain. When heating up, the interplanar distance changes due to the reversible thermoelastic expansion and due to the irreversible relaxation

$$d(T) = d_{ad} + \Delta d_{rev}(T) + \Delta d_{irr}(T) \quad (2)$$

where d_{ad} is the out-of-plane interplanar distance of the as-deposited film at room temperature, $\Delta d_{rev}(T)$ the reversible thermoelastic expansion and $\Delta d_{irr}(T)$ the irreversible change due to relaxation. The reversible change is $\Delta d_{rev}(T) = d_{ad}\alpha_{thel}\Delta T$. Now we define the reference value as $d(T,0) = d_{ad}(1+ \alpha_{thel}\Delta T)$. To determine $d(T,0)$ we take the thermoelastic expansion coefficient from the slopes in Fig. 3 and d_{ad} is known from the experiment before annealing starts. Using this reference value the residual strain, $\varepsilon(T,t)$, during in situ annealing at a temperature T is proportional the irreversible change of the out-of-plane interplanar distance

$$\varepsilon(T,t) = \frac{d(T,t) - d(T,0)}{d(T,0)} = \frac{\Delta d_{irr}(T,t)}{d_{ad}(1+\alpha_{thel}\Delta T)}. \quad (3)$$

Using the thermoelastic expansion coefficient we can determine the residual strain modification as a function of annealing time from our experimental data. Fig. 4 shows the residual strain for magnetron sputtered and ion beam sputtered Pt films during in situ annealing at 130 °C and 180 °C. One striking difference between the two types of Pt films is that the change of residual strain during in situ annealing is significantly higher in the case of the magnetron sputtered Pt films.

Another eye-catching difference is the shape of the Bragg peaks as given in Fig.1. Thickness fringes around the (111) Bragg peaks are characteristic for magnetron sputtered films. As can be seen from Fig. 1, such fringes are already present for the as-deposited films and become more pronounced after annealing. They allow us to determine the out-of-plane diameter of the

grains responsible for the thickness fringes and to estimate the out-of-plane grain size distribution for this type of films. As can be found in text books (e.g. [13]) in kinematic approximation the intensity I of a Bragg peak for a stack of N parallel atomic planes perpendicular to the scattering vector $\boldsymbol{q}$ is:

$$I = A^2 \frac{1-\cos(Ndq_z)}{1-\cos(dq_z)}. \quad (4)$$

Here, A is the amplitude of the scattered wave, $q_z = 4\pi\sin(\Theta)/\lambda$ is the normal component of the scattering vector, Θ the Bragg angle and λ the wave length. The thickness of the stack of atomic planes is Nd. The positions of the maxima and the minima of the thickness fringes are controlled by Nd. Since the out-of-plane interplanar distance, d, can be determined from the position of the Bragg, the parameter Nd allows us to estimate the number of coherently scattering planes, N. The positions of the minima are well resolved after the first annealing step and sufficiently resolved for the as-deposited samples. Using Eq. (4) we can simulate the pattern of the Bragg peak. An example is shown in Fig. 5a. From the simulation N or Nd can be determined quite accurately. Fig. 5b shows the same Bragg peak. Simulations for $N \pm 3$ lead to clear shifts of the positions of the fringes with respect to the measured data. Therefore, an error limit of the number of coherently scattering planes of $\Delta N \approx 3$ can be estimated which corresponds to an error limit of the thickness of $\Delta(Nd) \approx 7$ Å . The out-of-plane grain size of $Nd = (202 \pm 7)$ Å is equal to the thickness, $L = 203.6 \pm 0.1$ Å, of the film as measured by X-ray reflectometry (not shown), which does not change during in situ annealing. This means that for magnetron sputtered Pt films a significant number of (111) oriented columns is present which cover the whole film thickness. Eq. 4 is derived for a single stack of atomic planes. In our experiments we measure the incoherent superposition of coherently scattering columns: $I_{\mathrm{mesured}} = \Sigma I_{\mathrm{i}}$ where I_i are the intensities of the coherently scattering stacks. If the number of atomic planes is not equal for each stack the incoherent superposition leads to a damping of the oscillations. The quantity Nd which is deduced from the simulations is the

mean value of the out-of-plane size of the (111) oriented columns. A sharp size distribution of equally oriented grains is a prerequisite that thickness fringes are visible in the pattern of the Bragg peak. The well resolved fringes around the (111) Bragg peaks indicate that the out-of-plane grain size distribution of the magnetron sputtered films has a sharp maximum at $Nd \approx L$.

In the case of the magnetron sputtered Pt films, thickness fringes are present around the (111) Bragg peaks for the as-deposited samples which means that magnetron sputtering leads to Pt films which are predominantly composed of (111) oriented columnar grains covering the whole film thickness. In the case of ion beam sputtered Pt films, neither thickness fringes are present around the (111) Bragg peak of the as-deposited samples nor do thickness fringes emerge during annealing. This indicates that ion beam sputtering leads to a different out-of-plane grain size distribution in Pt films. The absence of thickness fringes around the (111) Bragg peak in the case of ion beam sputtered Pt films does not exclude a preferential orientation of the grains. Therefore, we performed EBSD measurements for both types of Pt films. Fig. 6 shows the inverse pole figures extracted from the measurements. Both types of films exhibit a (111) texture. The texture is present in the samples as-deposited (Fig. 6a and Fig. 6c) and becomes somewhat stronger after annealing at 210 °C (Fig. 6b and Fig. 6d). In the case of the magnetron sputtered Pt films the texture is significantly more pronounced. EBSD measurements confirm the strong (111) texture of the magnetron sputtered films. A major difference in the microstructure of the two types of Pt films is the different out-of-plane grain size distribution which is obvious from the presence respectively absence of thickness fringes around the (111) Bragg peak.

In the case of magnetron sputtered films, annealing leads to an increase of the intensity of the (111) Bragg peak (see Fig. 1). Fig. 7 shows the integrated area of the Bragg peak normalized to the initial value with respect to the annealing time. For magnetron sputtered samples, annealing leads to a maximum increase of the integrated area of about 10% at 130 °C and of

80 % at 210 °C. For the ion beam sputtered samples the increase of the integrated area is less than 5 % even at an annealing temperature of 210 °C.

In order to explain the intensity increase of the Bragg peak as shown in Fig. 7, we refer to previous work as given in ref. [14]. In ref. [14] we performed quasi simultaneous X-ray diffraction measurements in Θ/2Θ geometry and in grazing incidence geometry, respectively. The Pt films investigated in [14] had a thickness of about 40 nm and were produced via magnetron sputtering under the same conditions as the magnetron sputtered Pt films in this work. During in situ annealing the intensity of the (111) Bragg peak measured in Θ/2Θ geometry increases while the intensity of the (111) Bragg peak measured in grazing incidence geometry decreases [14]. This was interpreted as a reorientation of atomic planes [14]: during in situ annealing the amount of (111) oriented atomic planes parallel to the sample surface increases at the expense of the amount of (111) planes inclined towards the sample surface. In [14] reorientation of atomic planes was attributed to growth of (111) oriented grains. Grains with (111) orientation which are present in the as-deposited films grow at the expense of grains with different orientations. Therefore, in this work we measured the (111) Bragg peak for a magnetron sputtered sample as-deposited and after annealing at 210 °C in Θ/2Θ geometry as well as in grazing incidence geometry with an incidence angle of 0.5 ° (not shown). The intensity of the (111) Bragg peak measured in Θ/2Θ geometry is increased after annealing while the intensity of the (111) Bragg peak measured in grazing incidence geometry is decreased. From this we conclude that reorientation of atomic planes significantly contributes to the increase of the intensity of the (111) Bragg peak as shown in Fig. 7. In contrast to the magnetron sputtered films, the intensity of the (111) Bragg peak for the ion beam sputtered Pt films increases only slightly during in situ annealing. At 210 °C the increase is less than 5% (Fig. 7). Thermally induced grain growth in coarse grained metals is expected to take place at higher temperatures than 200 °C. However, molecular dynamics studies reveal that grain rotation, grain boundary sliding and grain boundary migration

(promoting grain growth) occur in nanocrystalline metals even at room temperature [15]. For an understanding of grain growth in thin films produced via sputter techniques we have to distinguish carefully between processes which take place during deposition of the film and those which take place during post-annealing after deposition. The main stages during deposition of thin metal films produced via sputter techniques are: nucleation, growth, coalescence and thickening [16]. Nuclei are agglomerations of atoms with definite crystallographic orientation. They grow as islands with a spherical shape [16]. If islands have grown to the point of contact coalescence occurs and a grain boundary is built to reduce surface energy [16]. A continuous film is fully coalesced and further deposition leads to a thickening of the film [16]. The microstructures of thin films evolve during film deposition [17] and depend significantly on the deposition parameters [18]. During nucleation, no orientation-selection is expected [16]. However, grains with minimum surface and interface energies can grow with higher rates [19]. In fcc metals (111) planes have a minimum surface energy for free surfaces and interfaces with nonreacting substrates [19] and a (111) texture can evolve. In fact a strong (111) texture is observed in thin Au films [19]. The films were deposited on oxidised silicon wafers at room temperature. The strong (111) texture was ascribed to a surface-energy-driven secondary grain growth (SEDSGG) [17]: (111) oriented grains grow at the expense of grains with different orientations. The growth of (111) oriented grains begins during deposition when the film thickness reaches about 17.5 nm [19]. The in-plane diameters of the secondary grains grow with increasing film thickness and exceed the thickness of the film [19]. In the stage of deposition before secondary grains are built the grains obey a log-normal distribution [20]. After the onset of SEDSGG the log-normal distribution is superimposed by the distribution of the secondary grains and a bimodal grain size distribution develops [19].

In our experiments, the thickness fringes around the (111) Bragg peak indicate the presence of (111) oriented grains covering the whole film thickness in the as-deposited magnetron

sputtered Pt films. However, TEM investigations on magnetron sputtered Pt films [21] deposited under the same conditions as in this work give no indication for secondary grains as observed in Au films. This holds true for Pt films as-deposited as well as for Pt films post-annealed at 130 °C for several hours [21]. Due to the higher melting point of Pt compared to Au the mobility of the grain boundaries is much lower at room temperature. Therefore, grain growth at the expense of other grains is supressed during deposition at room temperature. The strong (111) texture arises rather from a higher growth rate of the (111) oriented grains during deposition. Due to the minimum surface energy, the increase of the in-plane diameter of (111) oriented grains during deposition is higher than for other grains. This leads to a conical shape of the (111) orientated grains with the tip at the interface and the base at the surface. Columnar grains with a conical shape are typical for thin metal films [16].

Now we have a look at the situation during post-annealing: grain growth at the expense of other grains can occur during post-annealing. At temperatures of 180 °C – 210 °C the homologous temperature of Pt is comparable to the homologous temperature of Au at room temperature (melting point of Pt: 2041 K [10], melting point of Au: 1337 K [10]). In the case of the magnetron sputtered Pt films the strong increase of the intensity of the (111) Bragg peak as shown in Fig 7 can be attributed to surface-energy-driven in-plain grain growth. Grain growth is associated with a reduction of free volume in the film which leads to decrease of compressive stress [2,3]. Therefore, considerable relaxation of residual out-of-plane strain in magnetron sputtered Pt films as shown in Fig 4 is a consequence of in-plain grain growth during post-annealing.

In principle the increase of the Brag peak area as shown in Fig. 7 can be qualitatively also explained by a decrease of microstrain present in the nanocrystalline film. Microstrain results from a distribution of interplanar distances within a grain and should not be confused with residual strain shown in Fig 4. Residual strain leads to a shift of the Bragg peak while microstrain leads to a broadening of the Bragg peak. Microstrain can be determined from

XRD data using e.g. Williamson-Hall analysis. In our textured Pt films, however, only the (111) peak can be resolved sufficiently and no reliable results can be achieved from Williamson-Hall analysis. However, our experiments using different geometries and the results in ref. [14] show that relaxation of microstrain is not the dominating contribution here.

In contrast, in the case of ion beam sputtered Pt films (Fig. 7) only a slight increase of the intensity of the (111) Bragg peak can be observed during post-annealing. This means that only a slight growth of (111) oriented grains takes place during post-annealing of this type of Pt films. Minor grain growth means minor reduction of free volume and therefore minor reduction of compressive stress. Low relaxation of residual out-of-plane strain during post-annealing of ion beam sputtered films as shown in Fig. 4 can be ascribed to low grain growth. In contrast to the magnetron sputtered Pt films, no fringes around the (111) Bragg peak are observed in the case of ion beam sputtered Pt films. As already mentioned above, this indicates that the microstructure of the ion beam sputtered Pt films is different from the microstructure of the magnetron sputtered Pt films. The main difference between the two sputter techniques is that the deposition rate is significantly higher for magnetron sputtering (see section 2). General considerations yield that a low deposition rate promotes (111) texture in fcc metals [22]. A detailed study on the influence of deposition parameters on the microstructure of magnetron sputtered thin Pt films is given in reference [23]. Confirming the general considerations in [22] the investigations reveal that (111) texture increases with decreasing deposition rate [23]. Sputtering power and working pressure used for magnetron sputtering in our experiments were at the lower limit of the values used in [23]. The fact that the (111) texture is significantly weaker for the Pt films deposited with a significantly lower deposition rate is seemingly in contradiction to the findings in references [22, 23]. However, at a given sputtering power the columnar structure changes to a more granular structure of the grains if the deposition rate is decreased [23]. The deposition rate achieved by ion beam sputtering in our experiments is more than an order of magnitude lower than in the case of

magnetron sputtering. A possible explanation for the different microstructures might be that the low deposition rate achieved by ion beam sputtering in our experiments is not sufficient for the development of a columnar structure in the Pt films and therefore a weaker (111) texture evolves. However, further investigations are needed to clarify the influence of deposition parameters on the microstructure of sputter deposited Pt films.

It has to be noted, that in ref. [21] relaxation of compressive strain in 40 nm thin nanocrystalline Pt films in situ annealed at 130 °C was attributed to the generation of vacancies at the free surface of the film. According to Fig. 7 this is not in contradiction to our results here. At 130 °C the change of the Bragg peak intensity is rather limited, which means that grain growth is not the dominating contribution at this low temperature. Nevertheless, both mechanisms might contribute to relaxation of residual stress with a different dominance at different temperatures.

In conclusion, (111) oriented columnar grains covering the whole film thickness develop in thin Pt films during deposition via magnetron sputtering. Post-annealing leads to relaxation of residual out-of-plain strain. Both, the development of columnar grains during deposition and relaxation during post-annealing are driven by minimization of surface energy. In contrast no predominant (111) oriented grains covering the whole film thickness develop during deposition via ion beam sputtering where the sputter rate is significantly lower compared to magnetron sputtering. As a consequence minor relaxation of residual out-of-plane strain is observed during post-annealing for this type of films. An open question is which mechanism lies behind the reorientation of atomic planes in the case of magnetron sputtered Pt films. To clarify this question further experiments including advanced microscopic techniques are necessary.

5. Summary

In this study we compared strain relaxation in thin Pt films produced by different techniques - magnetron sputtering and ion beam sputtering. The Pt films with a thickness of about 20 nm were deposited on oxidised silicon wafers. We performed time dependent XRD measurements in Θ/2Θ geometry using synchrotron radiation. The (111) Bragg peak was measured during isothermal annealing at temperatures between 130 °C and 210 °C. For both types of films the out-of-plane interplanar distance decreases with increasing annealing time until a final value is reached. The decrease of the out-of-plane interplanar distance is stronger for higher temperatures. In situ annealing was performed until no significant change of the out-of-plane interplanar distance could be detected. After cooling down to room temperature the out-of-plane interplanar distance was determined again. The thermoelastic expansion coefficient was determined from the difference of the fully relaxed interplanar distance and the interplanar distance determined after cooling down to room temperature. The residual out-of-plane strain was determined using the thermoelastic expansion coefficient. In the case of the magnetron sputtered Pt films the decrease of residual out-of-plane strain at a given temperature is significantly higher than in the case of the ion beam sputtered films. According to a biaxial stress model this means that more compressive stress is relaxed in the case of the magnetron sputtered films. The microstructures of the two types of films are found to be significantly different. Thickness fringes are present around the (111) Bragg peaks of the as-deposited films produced via magnetron sputtering and become more pronounced during annealing. This clearly indicates that the films are predominantly composed of (111) oriented columnar grains with a sharp out-of-plane size distribution. From the positions of the minima of the thickness fringes an out-of-plane size of about 20 nm for the columnar grains was determined. This means that the columnar grains cover the whole film thickness. In contrast, no thickness fringes can be observed around the Bragg peaks of the ion beam sputtered Pt films. This holds true for the samples as-deposited as well as for the annealed samples. The (111) oriented columns covering the whole film thickness develop during magnetron sputtering. This

development is driven by surface energy minimization. Post-annealing leads to growth (111) oriented grains at the expense of grains with a different orientation and is also driven by surface energy minimization. The strong relaxation of residual out-of-plane strain is a consequence of grain growth. No predominant (111) grains covering the whole film thickness develop during ion beam sputtering and only slight growth of (111) oriented grains occurs during annealing after deposition. The slight relaxation of residual out-of-plan strain is a consequence of the slight grain growth. The different relaxation of residual out-of-plane strain in the two types of Pt films is ascribed to the different microstructures which evolve during deposition.

Acknowledgements

This work is based on measurements carried out at the Rossendorf beam line (BM20) at ESRF, Grenoble. We acknowledge the European Synchrotron Radiation Facility for provision of synchrotron radiation facilities. We thank J. Rahn and F. Strauß for help with sample preparation and J. Binzen for assistance during in situ measurements. EBSD measurements were carried out at Clausthaler Zentrum für Materialtechnik. The installation of the FEI Helios NanoLab 600 was supported by the German Research Foundation (DFG) under the contract INST 189/165-1 FUGG.This research has been supported by the German Research Foundation (DFG) under the contract Schm1569/13-3.

[1] R. Abermann, R. Kramer, J. Mäser, STRUCTURE AND INTERNAL STRESS IN ULTRA-THIN SILVER FILMS DEPOSITED ON MgF_2 AND SiO SUBSTRATES, Thin Solid Films 52 (1978) 215-229.

[2] P. Chaudhari, Grain Growth and Stress Relief in Thin Films, J. Vac. Sic. Technol. 9 1 (1972) 520-522.

[3] M. F. Doerner, W. D. Nix, Stresses and deformation processes in thin films on substrates, Crit. Rev. Solid State Mater. Sci. 14 3 (1988), 225-268.

[4] R. C. Cammarata, SURFACE AND INTERFACE STRESS EFFECTS IN THIN FILMS, Progress in Surface Sciences 46 1 (1994) 1-38.

[5] R. C. Cammerata, Surface and interface stress effects on interfacial and nanostructured materials, Materials Science and Engineering A237 (1997) 180-184.

[6] R. C. Cammerata, T. M. Trimble, D. J. Srolovitz, Surface stress model for intrinsic stresses in thin films, J. Mater. Res. 15 11 (2000) 2468-2474.

[7] J. A. Floro, S. J. Hearne, J. A. Hunter, P. Kotula, E. Chason, S. C. Seel, C. V. Thompson, The dynamic competition between stress generation and relaxation mechanisms during coalescence of Volmer–Weber thin films, J. Appl. Phys. 89 9 (2001) 4886-4897.

[8] W.D. Nix, B.M. Clemens, Crystallite coalescence: A mechanism for intrinsic tensile stresses in thin films, J. Mater. Res. 14 8 (1999) 3467-3473.

[9] J. A. Thornton, J. Tabock, D. W. Hoffman, Intenal Stresses in Metallic Films Deposited by Cylindrical Magnetron Sputtering, Thin Solid Films, 64 (1979) 111-119.

[10] D. R. Lide, CRC Handbook of Chemistry and Physics, CRC Press, Boca Raton, 2012.

[11] D. R. Lide, CRC Handbook of Chemistry and Physics, CRC Press, Boca Raton, 2009.

[12] J. Merker, D. Lupton, M. Töpfer, H. Knake, High Temperature Mechanical Properties of the Platinum Group Metals, Platinum Metals Rev. 45 2 (2001) 74-82.

[13] E. Zolotoyabko, Basic Concepts of X-ray Diffraction, Wiley-VCH, Weinheim, 2014, p. 97.

[14] W. Gruber, S. Chakravarty, C. Baehtz, H. Schmidt, Structural Re-Organization Kinetics of Nano-Crystalline Pt Films During In situ Annealing, Defect and Diffusion Forum, 323-325 (2012) 149-154.

[15] D. Farkas, S. Mohanty, J. Monk, Strain-driven grain boundary motion in nanocrystalline materials, Materials Science and Engineering A 493 (2008) 33-40.

[16] C. V. Thompson, Structure Evolution During Processing of Polycrystalline Films, Annu. Rev. Mater. Sci., 30 (2000) 159 – 190.

[17] C. V. Thompson, R. Carel, Texture development in polycrystalline thin films, Mater. Sci. Eng. B, 32 (1995) 211 – 219.

[18] C. V. Thompson, R. Carel, Stress and Grain Growth in Thin Films, J. Mech. Solids, 5 (1996) 657 – 673.

[19] C. C. Wong, H. I. Smith, C. V. Thompson, Surface-energy-driven secondary grain growth in thin Au films, Appl. Phys. Lett., 48 (1986), 335 – 337.

[20] C. G. Granqvist, R. A. Buhrman, Ultrafine metal particles, J. Appl. Phys., 47 (1976) 2200 – 2219.

[21] W. Gruber, S. Chakravarty, C. Baehtz, W. Leitenberger, M. Bruns, A. Kobler, C. Kübel, H. Schmidt, Strain Relaxation and Vacancy Creation in Thin Platinum Films, Phys. Rev. Lett. 107 (2011) 265501(5).

[22] C. V. Thompson, On the grain size and coalescence stress resulting from nucleation and growth processes during formation of polycrystalline thin films, J. Mater. Res. 14 7 (1999) 3164 – 3168.

[23] G. Schmidl, J. Dellith, E. Kessler, U. Schinkel, The influence of deposition parameters on Ti/Pt film growth by confocal sputtering and the temperature dependent resistance behavior using SiO_x and Al_2O_3 substrates, Applied Surface Science, 313, (2014) 267 – 275.

Figure captions

Figure 1: (111) Bragg-Peak of a 20 nm Pt film as-deposited (solid line) and after annealing at 180 °C for 10 h and cooling down (dotted line) deposited via magnetron sputtering (a) and ion beam sputtering (b).

Figure 2: Out-of-plane interplanar distance of the (111) planes as a function of annealing time during in situ annealing at 130 °C (open squares) and 180 °C (full circles) for 20 nm Pt films deposited via (a) magnetron sputtering and (b) ion beam sputtering, respectively. The first data points at $t < 0$ as well as the last points after the interception of the abscissa refer to room temperature. The error bars are smaller than the symbols.

Figure 3: Thermoelastic strain with respect to the temperature change for ion beam sputtered samples (full circles) and magnetron sputtered samples (open squares). The linear fits were performed under the constraint $\varepsilon_{thel} = 0$ for $\Delta T = 0$.

Figure 4: Residual strain for the magnetron sputtered Pt films (full squares) and the ion beam sputtered Pt films (open squares) at 130 °C and for the magnetron sputtered Pt films (full circles) and the ion beam sputtered Pt films (open circles) at 180 °C.

Figure 5: (a) Bragg peak of a magnetron sputtered Pt film after annealing at 210 °C for 10 h (open squares) and a simulation (solid line) according to Eq. 4 for $N = 88$. (b) The same Bragg peak as in (a) (open squares) and simulations using different numbers of atomic planes, N. Given are the simulation of (a) which fits to the data for $N = 88$ (solid line) as well as simulation for $N - 3$ (broken line) and $N + 3$ (dotted line).

Figure 6: Inverse pole figures extracted from the EBSD measurements for a magnetron sputtered Pt film as-deposited (a), a magnetron sputtered Pt film after annealing at 210 °C (b), an ion beam sputtered Pt film as-deposited (c) and an ion beam sputtered Pt film after annealing at 210 °C (d). The code of intensity is given in (e).

Figure 7: Normalised integrated area of the (111) Bragg peak for magnetron sputtered Pt films (ms) annealed at 130 °C (solid squares), 180 °C (solid circles) and 210 °C (solid triangles) together with that of an ion beam sputtered Pt film (is) annealed at 210 °C (open triangles). The error bars are smaller than the symbols.

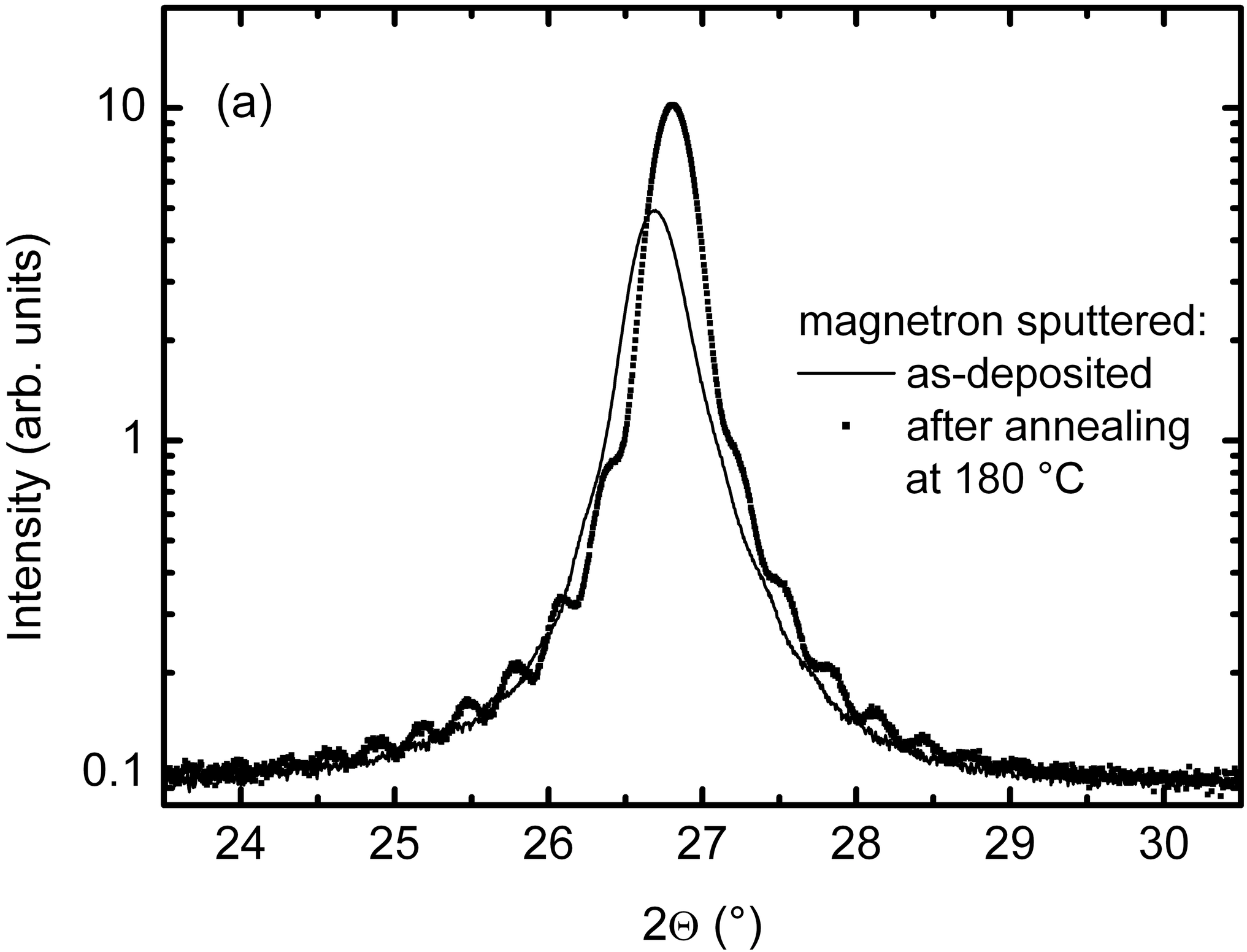
(a)
10
1
0.1
Intensity (arb. units)
24
25
26
27
28
29
30
2Θ (°)
magnetron sputtered:
as-deposited
after annealing
at 180 °C

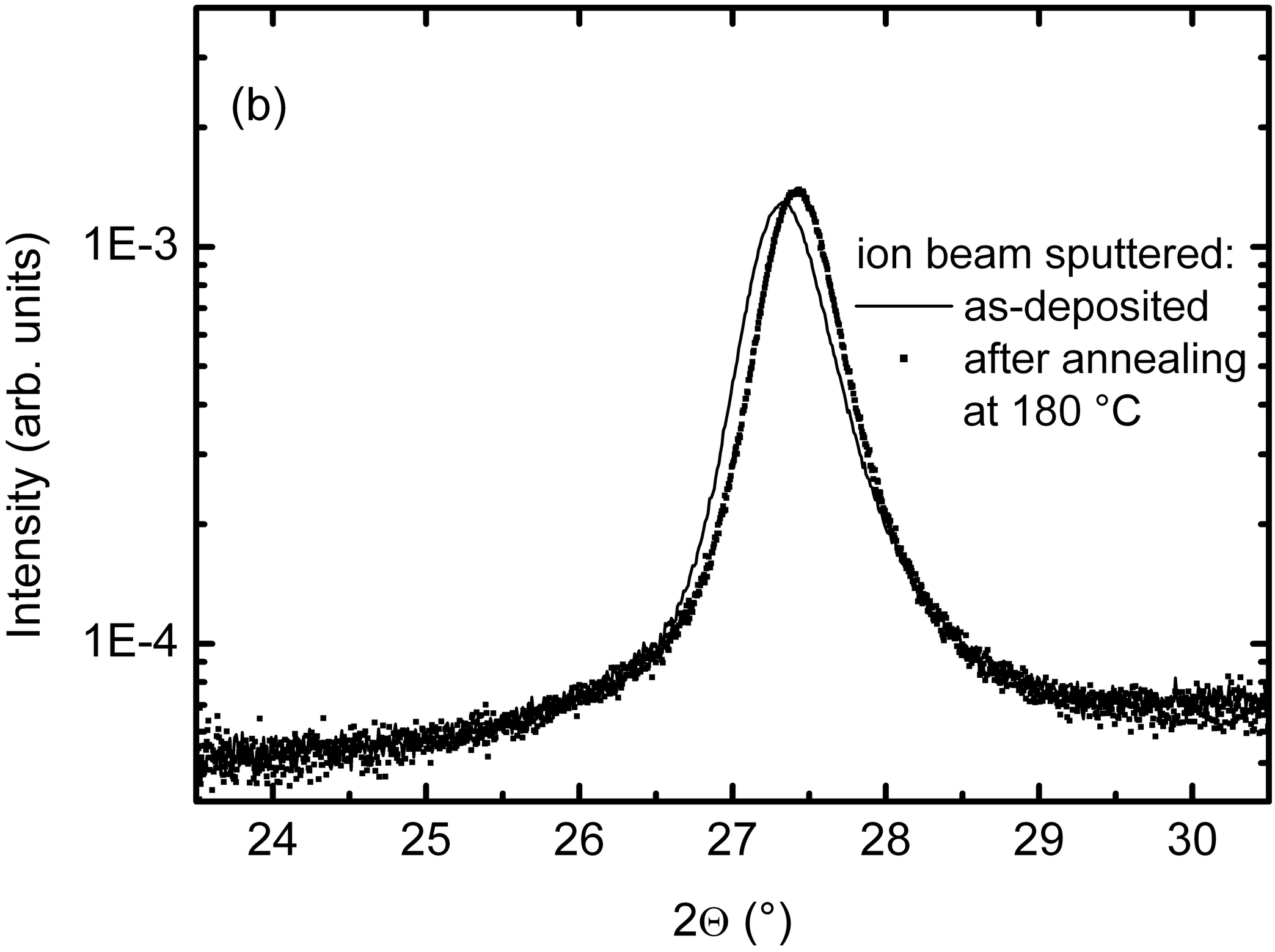
(b)
1E-3
1E-4
Intensity (arb. units)
ion beam sputtered:
as-deposited
after annealing
at 180 °C
24
25
26
27
28
29
30
2Θ (°)

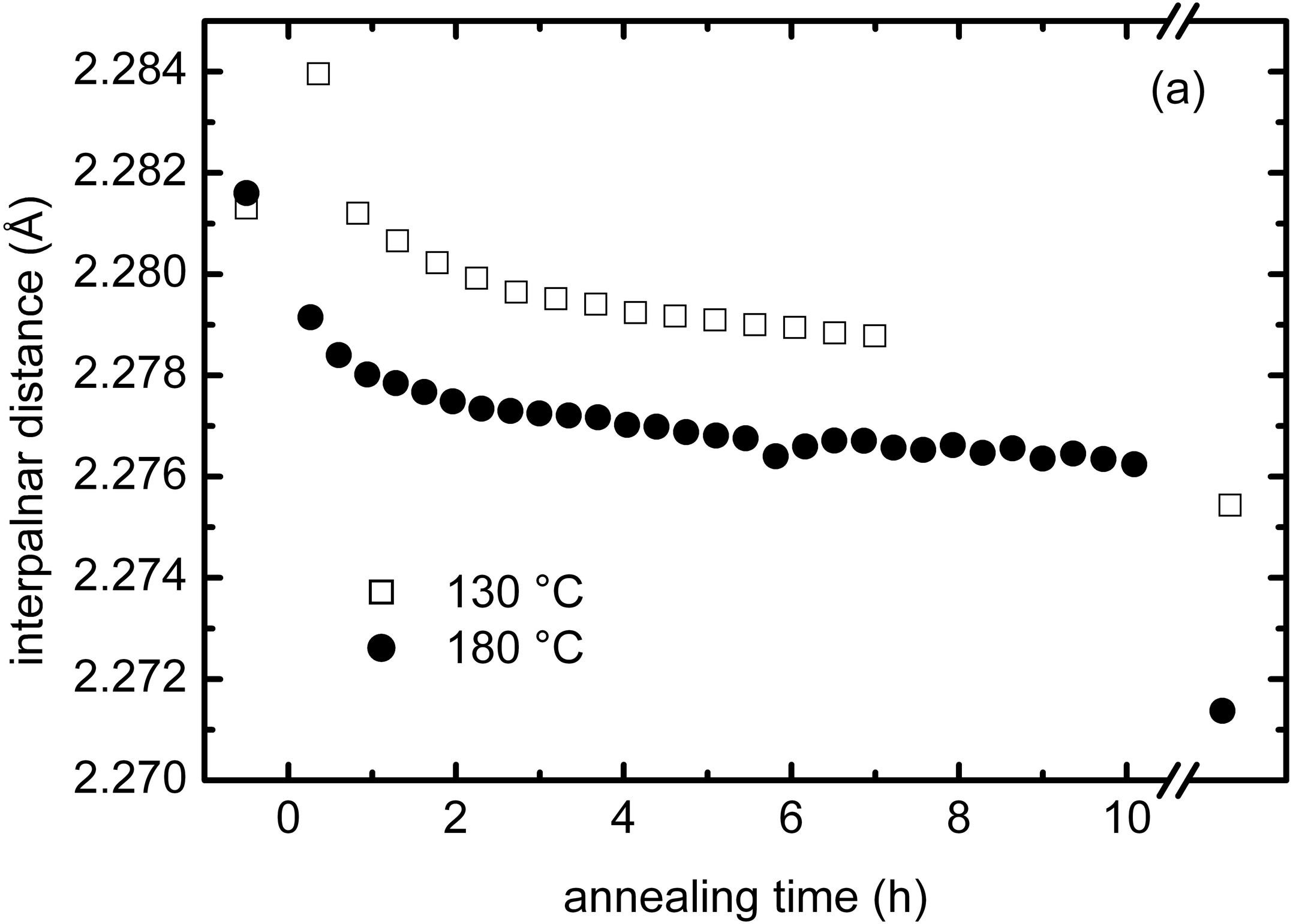
(a)
2.284
2.282
2.280
2.278
2.276
2.274
2.272
2.270
interpalnar distance (Å)
0
2
4
6
8
10
annealing time (h)
130 °C
180 °C

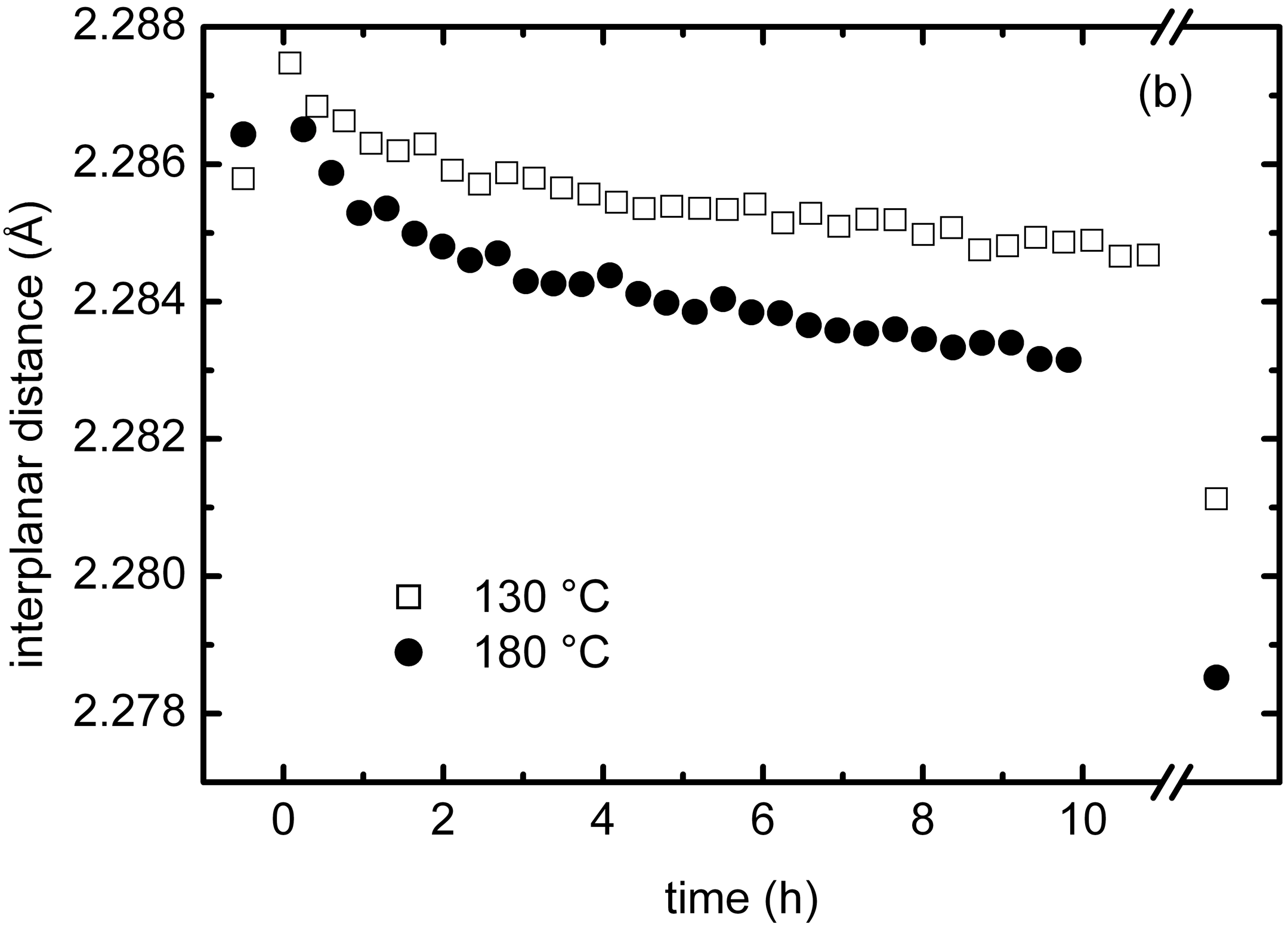
(b)
2.288
2.286
2.284
2.282
2.280
2.278
interplanar distance (Å)
130 °C
180 °C
0
2
4
6
8
10
time (h)

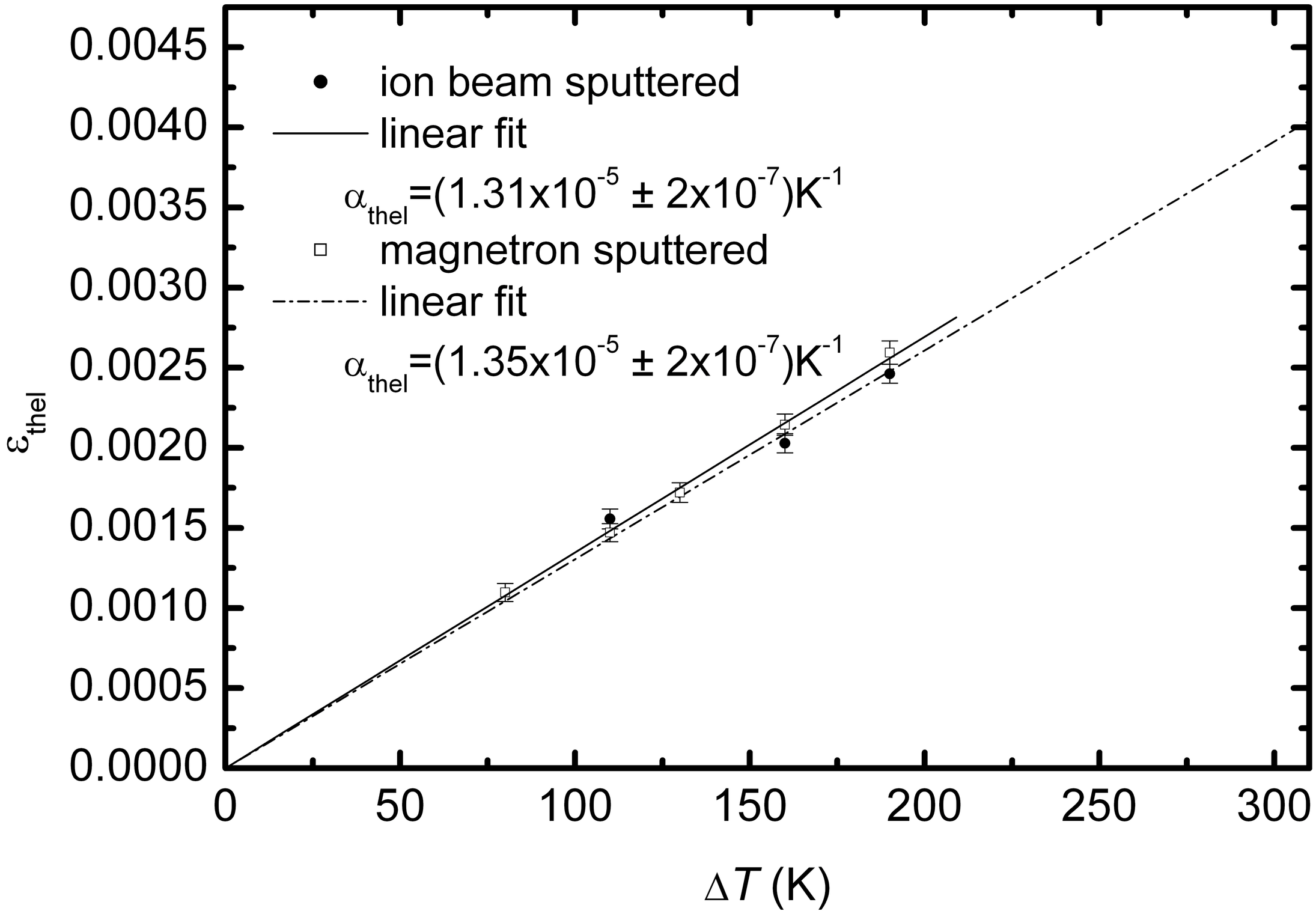
ion beam sputtered
linear fit
$\alpha_{thel}=(1.31x10^{-5} \pm 2x10^{-7})K^{-1}$
magnetron sputtered
linear fit
$\alpha_{thel}=(1.35x10^{-5} \pm 2x10^{-7})K^{-1}$
ε_{thel}
0.0045
0.0040
0.0035
0.0030
0.0025
0.0020
0.0015
0.0010
0.0005
0.0000
0
50
100
150
200
250
300
ΔT (K)

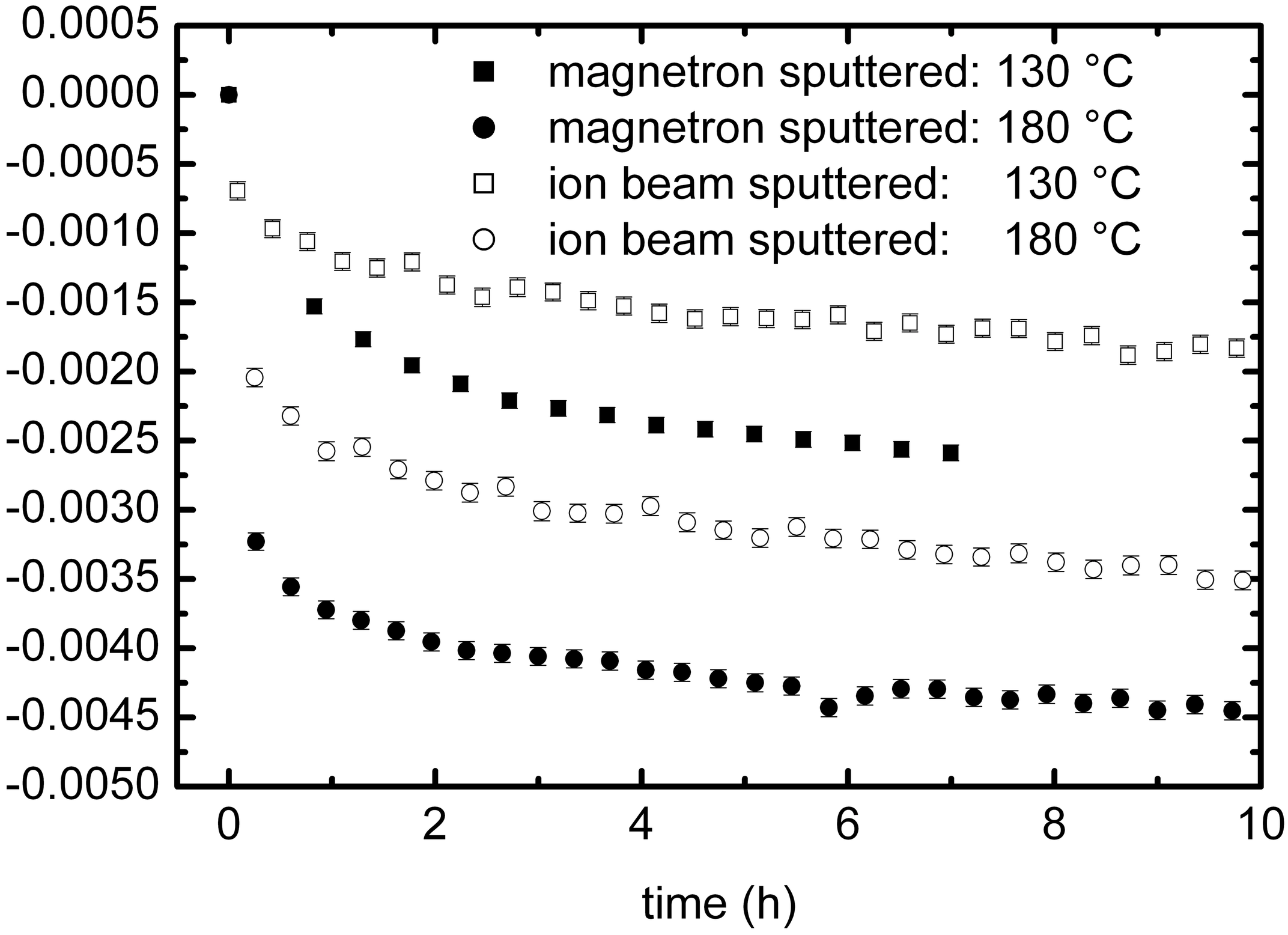
0.0005
0.0000
-0.0005
-0.0010
-0.0015
-0.0020
-0.0025
-0.0030
-0.0035
-0.0040
-0.0045
-0.0050
0
2
4
6
8
10
time (h)
magnetron sputtered: 130 °C
magnetron sputtered: 180 °C
ion beam sputtered: 130 °C
ion beam sputtered: 180 °C

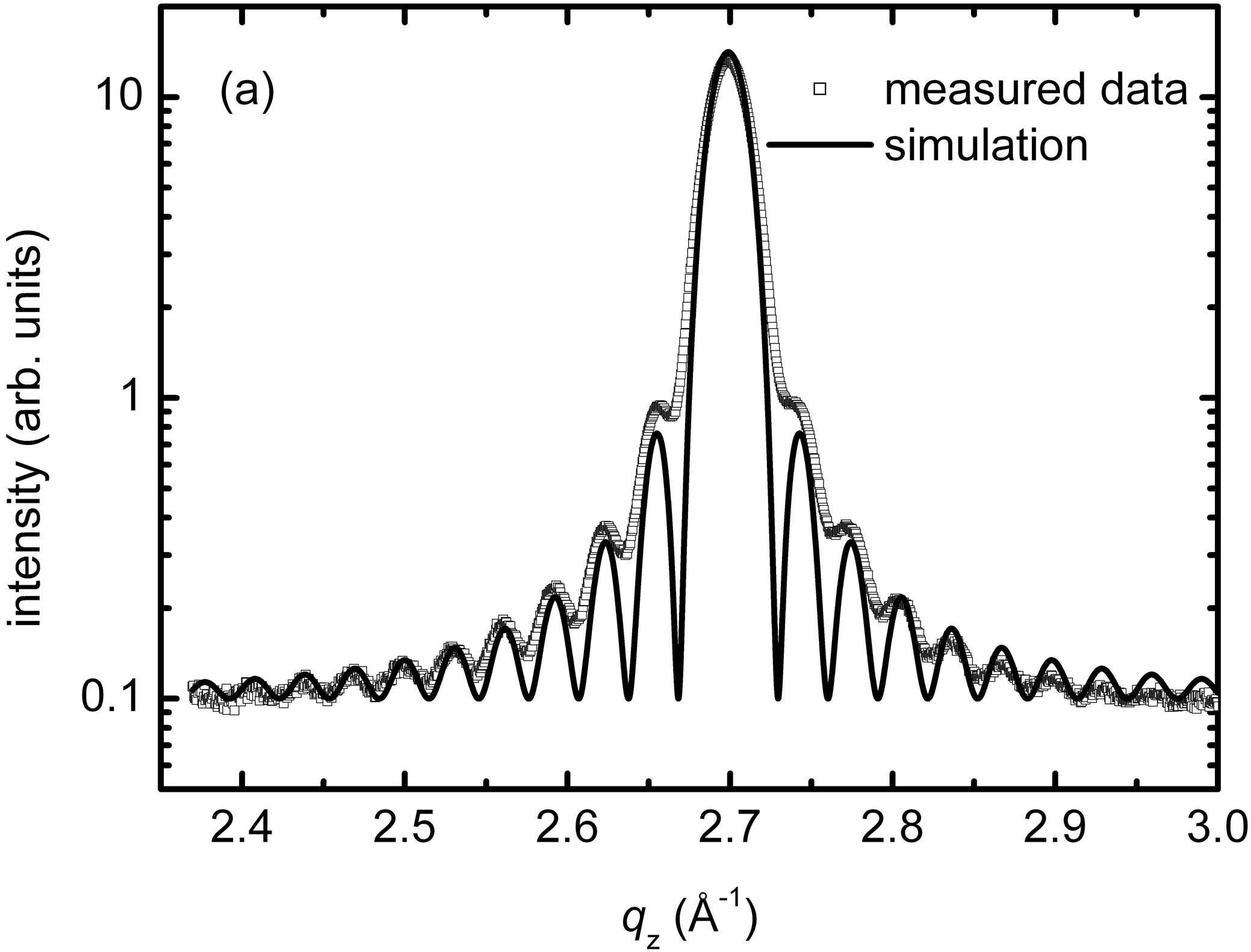
(a)
measured data
simulation
intensity (arb. units)
10
1
0.1
2.4
2.5
2.6
2.7
2.8
2.9
3.0
q_z (Å^{-1})

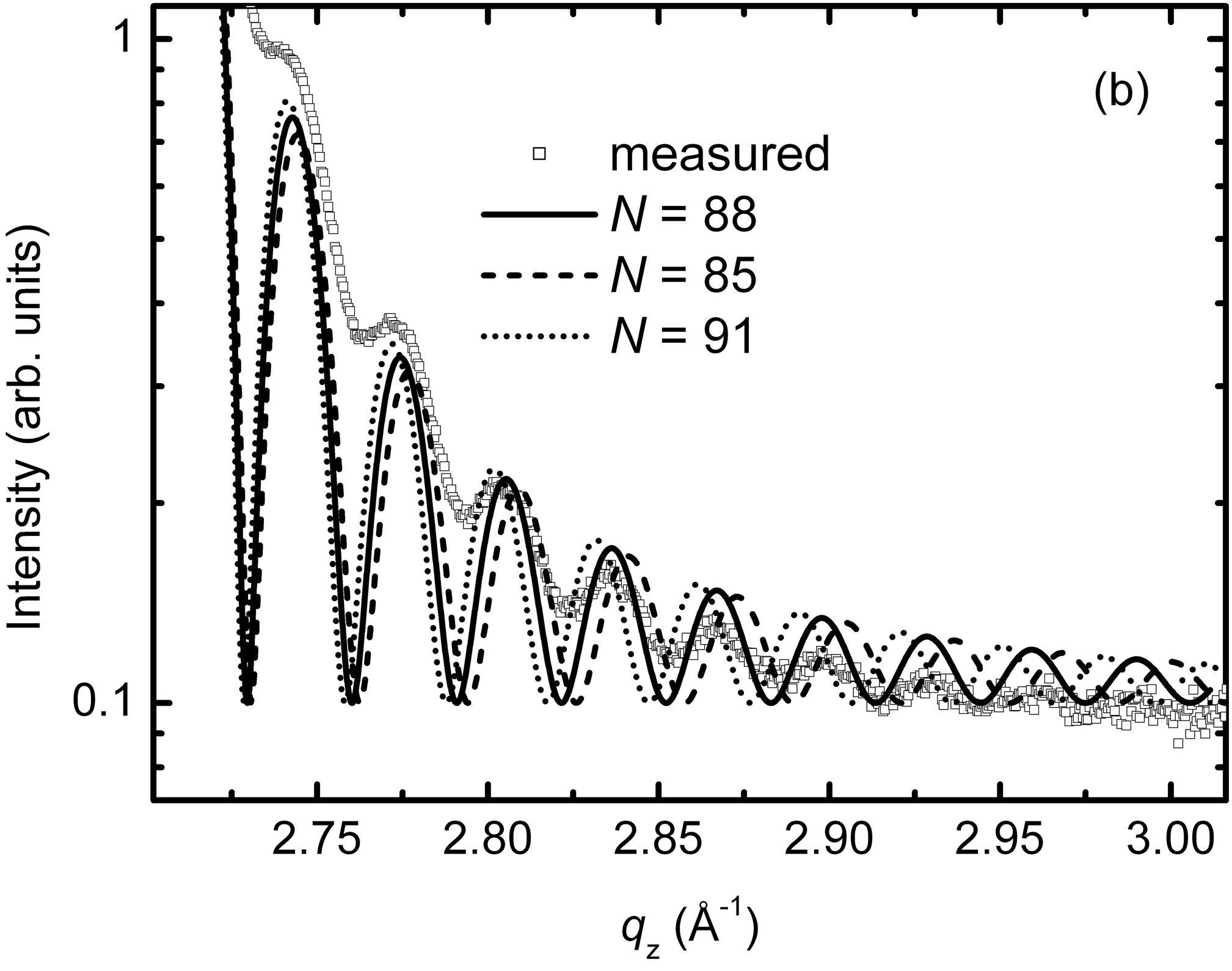
(b)
measured
N = 88
N = 85
N = 91
Intensity (arb. units)
1
0.1
2.75
2.80
2.85
2.90
2.95
3.00
q_z (Å^-1)

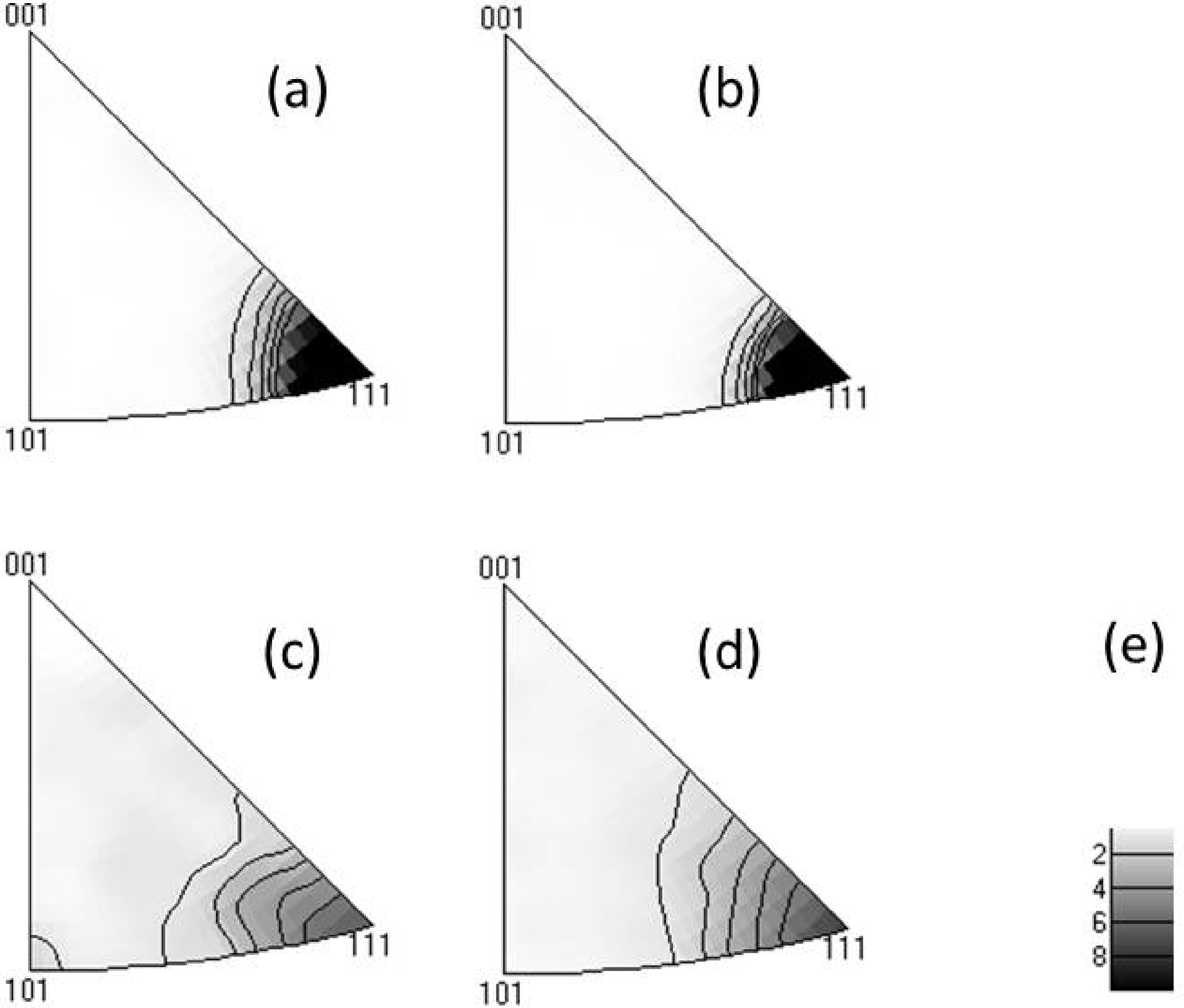
001
(a)
111
101
001
(b)
111
101
001
(c)
111
101
001
(d)
111
101
(e)
2
4
6
8

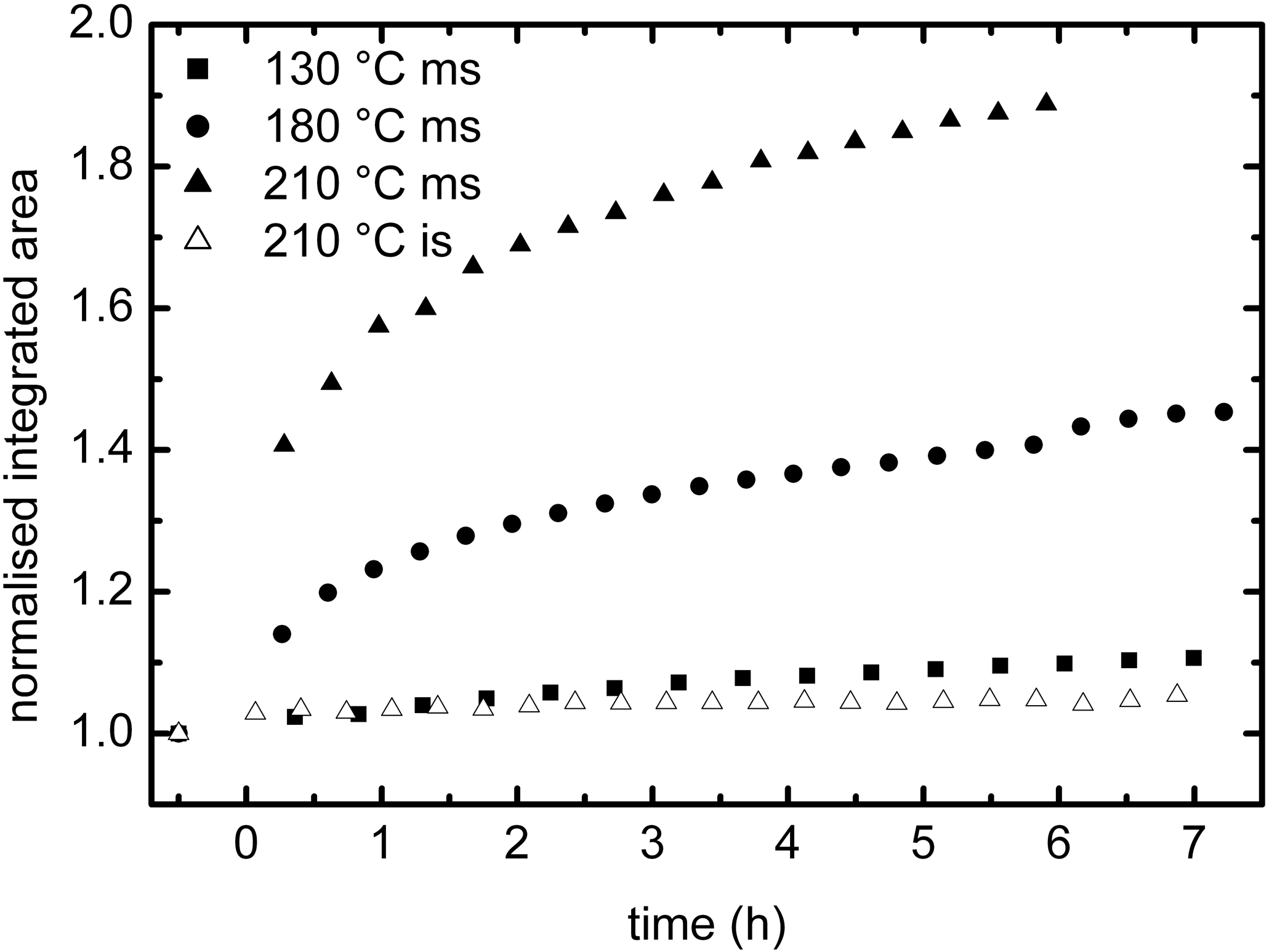
130 °C ms
180 °C ms
210 °C ms
210 °C is
normalised integrated area
2.0
1.8
1.6
1.4
1.2
1.0
0
1
2
3
4
5
6
7
time (h)

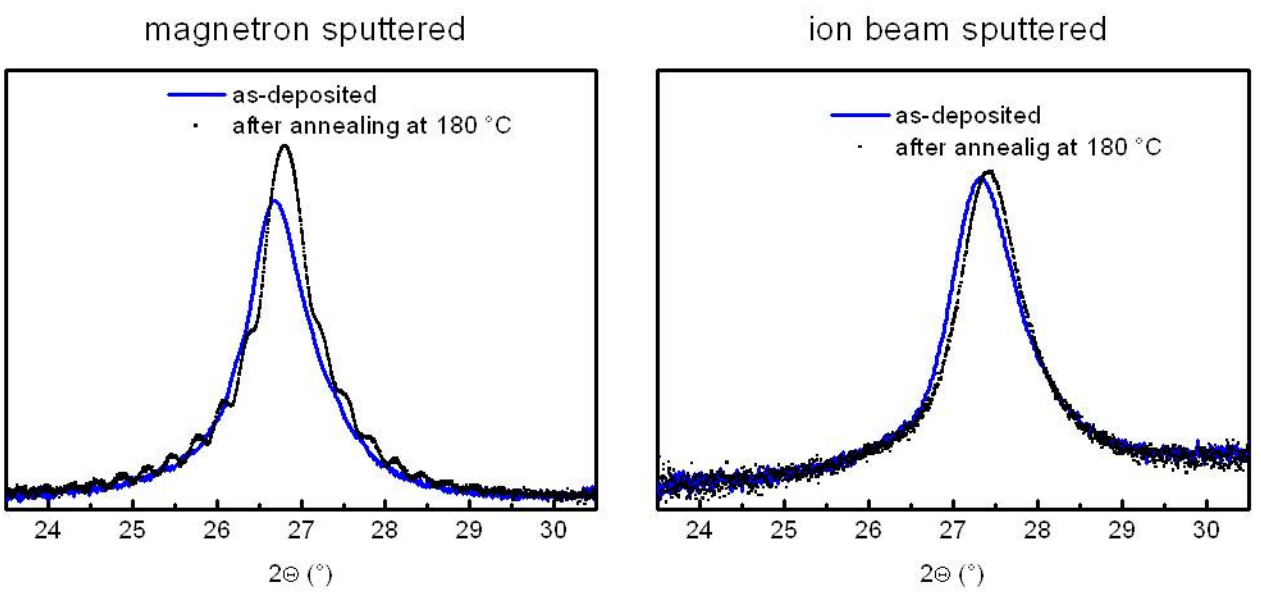
magnetron sputtered
as-deposited
after annealing at 180 °C
24
25
26
27
28
29
30
2Θ (°)
ion beam sputtered
as-deposited
after annealig at 180 °C
24
25
26
27
28
29
30
2Θ (°)